JOURNAL OF SPACECRAFT AND ROCKETS
Vol. 33, No. 4, July–August 1996

Three-Dimensional Modeling of Dual Ion-Thruster Plumes for Spacecraft Contamination

R. I. Samanta Roy* and D. E. Hastings†
Massachusetts Institute of Technology, Cambridge, Massachusetts 02139

The plume structure and the backflow of both propellant and sputtered grid material from two 8-cm xenon ion thrusters operating simultaneously were investigated with a three-dimensional model of an ion-thruster plume based on the plasma particle-in-cell technique. Thruster center to center separation distances of 10 and 17 cm were examined. The separation distance was found to play a strong role in determining the potential structure that affects propellant charge-exchange ion transport. Because of the combined potential structure of the two beams, the propellant charge-exchange ion backflow was found to be enhanced along an axis perpendicular to a line joining the thruster centers, whereas this was not the case for the more energetic sputtered molybdenum grid material. The implications of such asymmetry in the structure of the backstreaming flowfield from twin thrusters are important for thruster–spacecraft integration.

Nomenclature

A_g = sputtered grid area, m^2
A_n = grid neutral flow through area, m^2
$\bar{C}$ = neutral average value speed, m/s
e = electron charge, C
I_b = thruster beam ion current, A
j_{bi} = beam ion current density, A/m^2
k = Boltzmann's constant, mks
M = mass of grid lost due to sputtering over a period of time, kg
$\mathcal{M}$ = molecular weight, kg/mole
m_i = ion mass, kg
$\dot{m}_T$ = thruster total mass flow rate, kg/s
$\dot{N}_{cex}$ = charge-exchange (CEX) ion production rate, number/m^3/s
$\mathcal{N}_A$ = Avogadro's number
n_{bi} = beam ion density, m^{-3}
$n_{i,e,n}$ = total ion, electron, neutral density, m^{-3} (a further subscript 0 denotes reference)
$r_{b,T}$ = beam, thruster radius, m
T_e = electron temperature, K
T_w = thermal wall temperature of neutrals, K
v_{bi} = beam ion velocity, m/s
α = beam divergence angle, rad
Γ_s = sputtered grid material flux, number/m^2/s
η_p = propellant utilization efficiency
σ_{cex} = CEX cross section, m^2
τ = period over which grid mass is lost, s
Φ_b = beam acceleration voltage, V
ϕ = electric potential, V

Introduction

SPACECRAFT contamination by plume backflow from electric propulsion (EP) thrusters is a concern for spacecraft designers and integrators, just as it is for chemical propulsion.[1] With EP thrusters, however, the mixture of neutral gases, plasmas, and electromagnetic fields that results from interactions between the ambient space environment, thruster effluents, and the spacecraft itself produces a far more complex contamination environment. Recently, the plume backflow from ion thrusters has been investigated with both axisymmetric[2,3] and fully three-dimensional[4] numerical models. However, these studies examined the plume of a single thruster. In reality, thrusters will most likely be operated on spacecraft in multiples or at least in pairs for increased thrust, as well as reliability.

In this paper, we extend our three-dimensional single-thruster model to examine the plumes and backflow from two thrusters operating simultaneously. The most important issue is whether the backflow from each individual thruster can be superimposed to give the total backflow from a group of thrusters. The aim of this paper is to address this issue by showing that the backflow is indeed nonlinear. In this paper, we first briefly review the physical and numerical aspects of the model that have been presented in detail elsewhere.[2–4] Results and discussion are then presented, followed by conclusions.

Physical Model

The ion-thruster plume and backflow contamination model used in this study, detailed in Samanta Roy et al.[2,4] accounts for the five major thruster effluents: 1) fast (>10 km/s) propellant beam ions that provide the thrust; 2) un-ionized propellant neutrals with thermal energies that flow from both the discharge chamber and the neutralizer; 3) slow (initially thermal) propellant ions created predominantly from charge-exchange (CEX) collisions between the beam ions and neutrals; 4) nonpropellant efflux (NPE) that consists mainly of eroded grid material, typically molybdenum, of which a fraction is charged resulting from either CEX or electron bombardment ionization; and 5) electrons. In this section, brief descriptions of the five components are given. Some of the elements of the model are given in terms of axisymmetric coordinates for simplicity, but are implemented as fully three dimensional. The thruster propellant considered in this work will be the most common one currently in use, xenon.

CEX Propellant Ions

The most dominant components of the backflow from an ion thruster are initially thermal propellant ions that are created inside the beam(s) resulting from resonant CEX collisions between the fast beam ions and the slow thermal neutrals; i.e., for xenon

$$Xe^+_{fast} + Xe^0_{slow} \rightarrow Xe^+_{slow} + Xe^0_{fast} \quad (1)$$

Because of their low initial energies (~500 K), these ions are easily affected by local potential gradients within the plume. The spatial volumetric production rate of CEX ions is given by

$$\dot{N}_{cex}(\boldsymbol{x}) = n_n(\boldsymbol{x}) n_{bi}(\boldsymbol{x}) v_{bi} \sigma_{cex}(v_{bi}) \quad (2)$$

where the relative collision velocity is taken to be the beam ion velocity. For plume electron temperatures around 1–2 eV, common to

Received Aug. 2, 1995; revision received April 3, 1996; accepted for publication April 3, 1996.

*Postdoctoral Associate, Space Power and Propulsion Laboratory, Department of Aeronautics and Astronautics; currently Research Staff Member, Institute for Defense Analyses, Alexandria, VA 22311. Member AIAA.

†Professor, Space Power and Propulsion Laboratory, Department of Aeronautics and Astronautics. Associate Fellow AIAA.

xenon ion thrusters, CEX is the dominant ion production mechanism compared to electron impact ionization. For xenon, the CEX cross section for 1-kV ions is on the order of 10^{-19} m^2 (Ref. 5). In general, CEX production rates are low enough that the beam ion and neutral densities can be taken to be fixed quantities. An important issue is appropriate models for these densities with multiple beams.

Beam Ions

The velocity of the collimated beam ions that are accelerated by the thruster grids and provide the thrust is given by $v_{bi} = (2e\Phi_b/m_i)^{1/2}$. Typical beam acceleration voltages are around 1 kV, leading to velocities above 10,000 m/s. The radial current density profile of the collimated beam ions [given in cylindrical coordinates (r, x) for simplicity] can be approximated[6] well with a parabolic axisymmetric profile given by

$$j_{bi}(r, x) = \left(2I_b/\pi r_b^2\right)\left[1 - \left(r^2/r_b^2\right)\right] \tag{3}$$

where $r_b = r_T + x\tan\alpha$. Given the beam ion current density, the beam ion density is then determined by

$$n_{bi}(r, x) = \frac{j_{bi}(r, x)}{ev_{bi}} \tag{4}$$

The effect of doubly ionized ions is neglected since their density, depending on thruster operating conditions, is on the average, an order of magnitude less than the singly charged ions.

An important modeling issue regarding multiple thruster operation is the interaction between the beams. In the axial direction, the beams are costreaming, and in the radial direction, counterstreaming as they penetrate each other. The presence of streaming instabilities may give rise to fluctuating electric fields and turbulence that may affect the transport of slow thermal ions within the beam. In addition, beam instabilities will convert the kinetic energy of fast beam ions to thermal energy and will enhance plume spreading over some length scale. However, these kinetic effects can not be dealt with rigorously with the present model because of the fluid nature of the electron model. Such issues must be addressed with a fully kinetic model of both the ions and electrons within the beam which are currently under investigation.[7]

In the previous single-beam modeling, the beam ion density was given by an analytical expression which agreed well with experimental data. To model multiple thrusters, an important issue is whether the beam ion models can be superimposed for the multiple thrusters. This issue was addressed by comparing the CEX ion production rates based on adding the densities of two individual ion beams and a more rigorous method where the beam ions were treated as computational particles. In the latter method, beam ions were injected each time step from two thrusters, until the beams fully developed, i.e., the first particles traversed the computational domain. The volumetric CEX ion creation rates from the two approaches compared well, as shown in Fig. 1. In this figure, the number of CEX ions created by the injection method rises to a steady state when the beam fully develops. Slight differences were noted at the beam edges; the particle beam had a divergence angle that was greater by 1–2 deg, but in these regions, the amount of CEX ions created was negligible. Thus, the approach of simply adding the beam ion densities for the two beams is reasonable. A numerical model was developed that could be applied to any number of thrusters in any arbitrary geometric configuration as long as they are oriented in the same direction and their exit planes are the same. However, in this study, we only considered two thrusters. Unfortunately, very little data has been taken from dual thruster operation, so detailed comparisons are not possible. However, the numerical model applied to single thrusters gives good agreement.[2,6]

Neutral Model

Not all of the propellant is ionized within the ion thruster. The un-ionized gas effuses out from the discharge chamber, and exits through the grids in free-molecular flow with a temperature close to that of the thruster discharge chamber walls, typically around 500 K for thrusters using xenon. The neutral density field is modeled as the

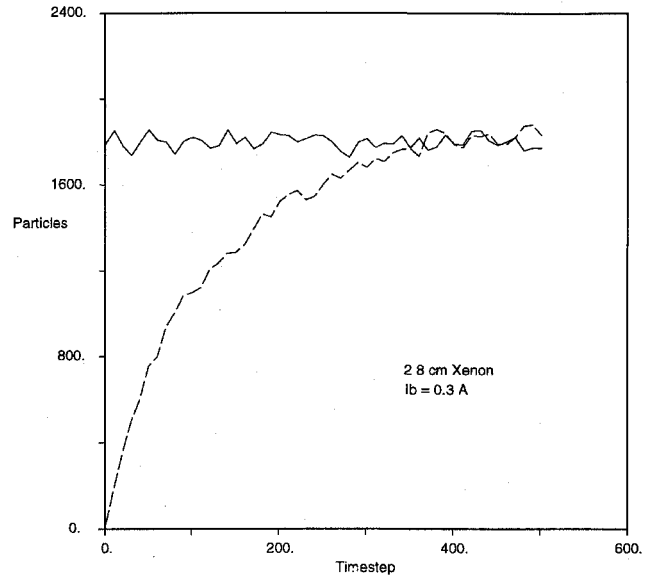

Fig. 1 Comparison of two CEX ion production rate methods with two thruster beams with beam ion particle injection and superposition of constant density models: ——, density model and – – –, particle beam.

flow from a single-point source that is located one thruster radius behind the exit plane of the grids. The neutral gas density is given by

$$n_n(R, \theta) = a(n_{n0}/2)\left\{1 - \left[1 + (r_T/R)^2\right]^{-\frac{1}{2}}\right\}\cos\theta \tag{5}$$

where $a = [1 - 1/\sqrt{2}]^{-1}$ is a correction factor to account for the shifting of the point source and $R = [r^2 + (x + r_T)^2]^{1/2}$, $\theta = \tan^{-1}[r/(x + r_T)]$. The average neutral density right at the thruster grids is determined from the beam ion current and the propellant utilization efficiency by $n_{n0} = 4I_b(1 - \eta_p)/e\bar{C}A_n\eta_p$, where $\bar{C} = (8kT_w/\pi m_i)^{1/2}$. The propellant utilization efficiency is based on the total neutral flow rate (discharge plus neutralizer) and is defined by

$$\eta_p = (I_b/\dot{m}_T)(m_i/e) \tag{6}$$

The neutral density from multiple plumes is taken to be the sum of the individual plumes since the neutral gas flow is collisionless.

NPE

Neutral molybdenum sputtered mainly from the accel grid can become ionized in the plume and flow back toward the spacecraft presenting a serious contamination hazard due to its low vapor pressure. Even a monolayer of molybdenum can cause serious degradation in the transmittance of solar cell coverglasses.[8] The molybdenum neutral density is computed from the sputtered material flux that is estimated from grid mass loss measurements. Given an amount of mass lost over a period of time, then the average flux is

$$\Gamma_s = (M/\tau A_g)(\mathcal{N}_A/\mathcal{M}) \tag{7}$$

The spatial distribution of the sputtered neutrals is assumed to be a cosine distribution as described by Eq. (5). The measured ejection energy distribution of molybdenum is found to be close to a Maxwellian speed distribution, and the density is determined by dividing the sputtered flux by the most probable ejection speed, which was taken to be around 3200 m/s (Ref. 9). The neutral molybdenum can become ionized via nonresonant CEX and by electron impact ionization collisions, the latter of which are more important, especially at electron temperatures above 1.5 eV.

Electrons

The hollow-cathode neutralizer, which is the most common on current ion thrusters, produces a quasineutral plasma cloud that acts as a bridge for the passage of electrons to the beam. In this paper, we treat these neutralizing electrons as an isothermal fluid with a drift velocity equal to the ion drift velocity. An analysis of the electron momentum equation leads to a balance between the pressure

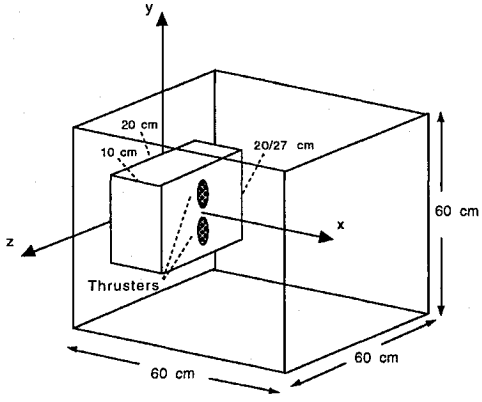

Fig. 2 Schematic of computational domain.

and electrical potential gradients. Hence, the appropriate description for the electron density is a Boltzmann distribution referenced to a specified background density,

$$n_e = n_{e\infty} \exp(e\phi/kT_e) \tag{8}$$

The electrons, as well as the ions, are unmagnetized in the model. The assumption of constant temperature leads to a more conservative estimate of the backflow compared to a variable temperature model and experiment.[6]

Numerical Implementation

Figure 2 shows a schematic of the computational domain with a model spacecraft and two thrusters located on the positive x-axis face. To model the expansion of the CEX ions, a hybrid electrostatic plasma particle-in-cell (PIC) technique is employed.[10] The PIC method follows the propellant CEX ions under the influence of self-consistent electric fields as they are transported out of the beam and form a plasma cloud that surrounds the spacecraft. The beam ion and neutral propellant models developed give the beam properties in the region of the plume, and the volumetric CEX propellant ion production model is used to determine the number of propellant CEX ions that are created per unit time per unit volume within the plume. The energies of the propellant CEX ions are drawn from a thermal Maxwellian distribution drifting downstream. The NPE ions are also created volumetrically, either by CEX or ionization at higher electron temperatures. However, since the NPE ion density is much smaller than the propellant plasma densities, the effect on the potential is negligible. Hence, the NPE plasma propagation is determined solely by ion tracking in the potential determined from the propellant CEX expansion. NPE ions are created with energies determined from an experimentally determined sputtering distribution[9] and are given a direction of motion in a line of sight from randomly chosen sputtering sites on the grids. Nearly 400,000 particles were used in the simulations.

The simulation is run until steady state is achieved when the number of particles within the domain becomes constant, i.e., the loss of particles at the boundaries and spacecraft surfaces balances the production rate within the plume. At steady state, the current backflowing to biased spacecraft surfaces resulting from propellant CEX and NPE ions can be computed, and assessments of surface deposition can be made. In this work, the surfaces are assumed to be absorbing. The nonlinear Poisson equation for the potential is solved throughout the computational domain. The outer boundaries shown in Fig. 2 are left open to space, although potentials can be fixed to simulate a ground testing chamber. All surfaces of the spacecraft are biased, either at fixed potentials or they are allowed to float as a single isolated conductor. A uniform background plasma density is assumed. Since the plasma environment produced by the thruster is orders of magnitude larger than the ambient, we ignore the dynamics of the background plasma over the length scales of interest.

Results

In this study, the plumes and backflow were investigated for two 8-cm beam diameter ion thrusters using xenon as propellant. Two thruster center to center separation distances were examined: 10 and 17 cm. The thrusters were oriented along the x axis, as in Fig. 2, on a model rectangular spacecraft that was 10 cm long in the x direction and 20 cm in the z direction. In the y direction, the spacecraft was 20 or 27 cm long corresponding to the two thruster separation distances. The computational domain was 0.6 m along each side. Each thruster had a beam current of 0.3 A, a beam velocity of 33,200 m/s, and a propellant utilization of 0.84. Ambient plasma conditions typical in low Earth orbit were used. For the sputtered molybdenum grid material, a neutral density of 3.25×10^{13} m^{-3} was used, which was a value based on measurements from a 30-cm xenon thruster.[3] The actual value used was only representative; the goal here was to explore qualitatively the distributions with two thrusters operating, and not to predict the backflow for a given thruster and thruster–spacecraft configuration.

Directional Orientation of Backflow

A unit vector plot in the x–y plane ($z = 0$) of the propellant CEX ion current density is shown in Fig. 3. This figure clearly shows the transport of the CEX ions, created within the beams, radially

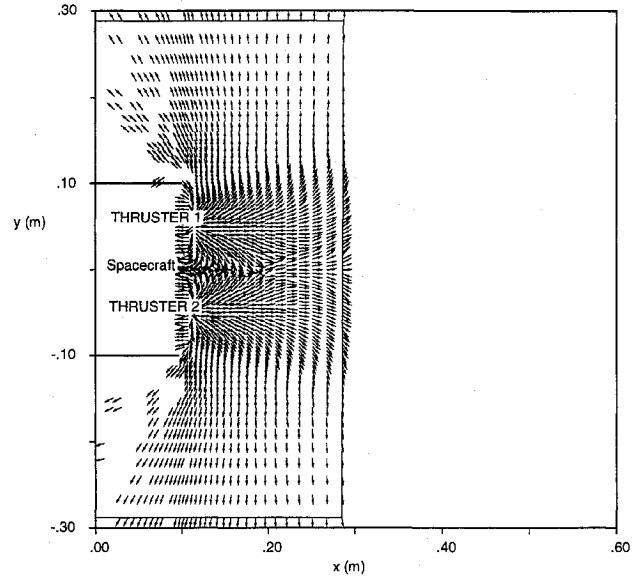

Fig. 3 Unit vector plot of propellant CEX ion current density in x–y plane (z = 0); dual thrusters; centerline separation of 10 cm (three-dimensional ion-thruster plume simulation).

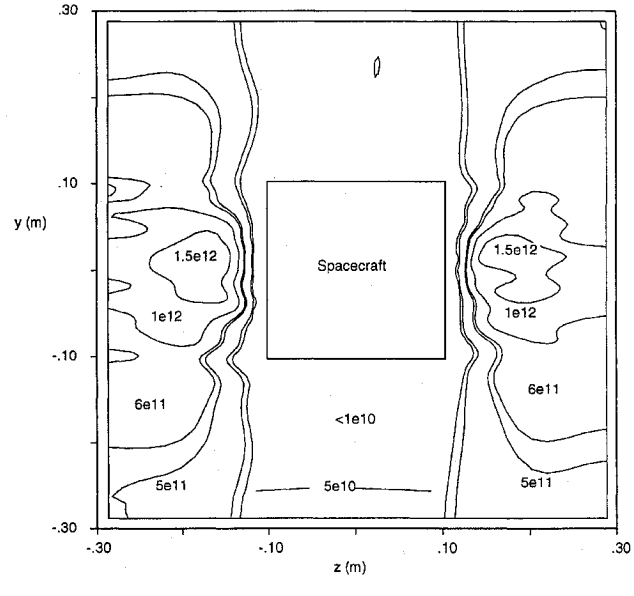

Fig. 4 Contour map of propellant CEX ion density in y–z plane 2 cm behind thruster exit plane (x = 8 cm looking downstream); dual thrusters; centerline separation of 10 cm (three-dimensional ion-thruster plume simulation).

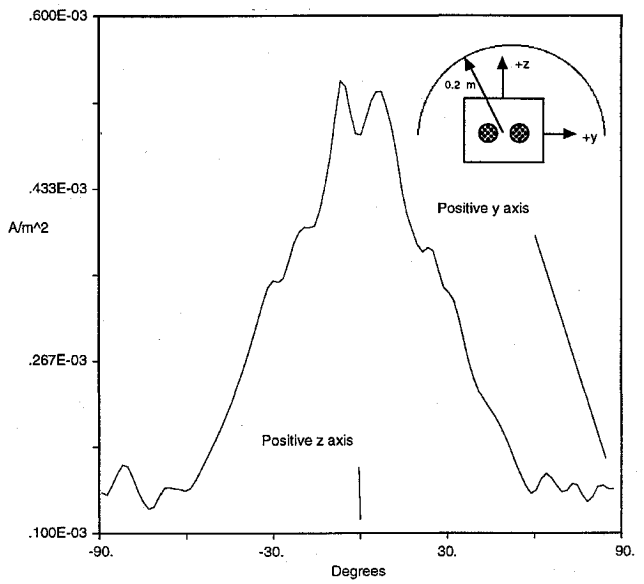

Fig. 5 Angular cut of propellant CEX ion density from $-y$ to $+y$ axis in same y–z plane as in Fig. 3; arc radius is 20 cm (three-dimensional ion-thruster plume simulation).

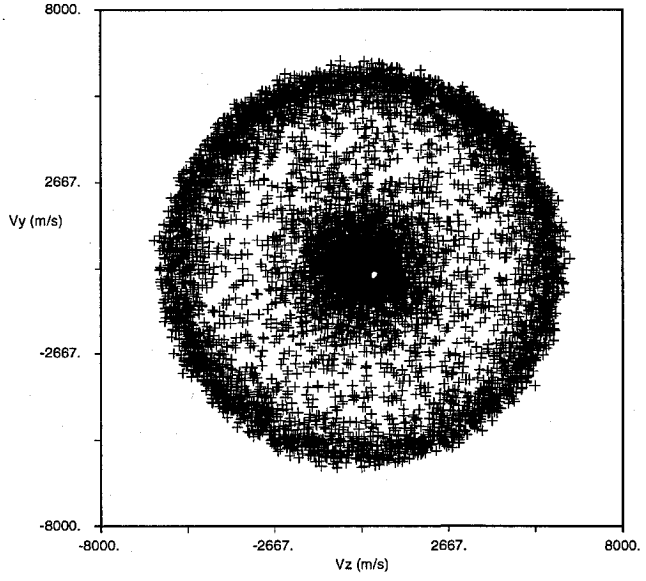

Fig. 6 Propellant CEX ions v_y–v_z velocity distribution plot for a single thruster (random subset of all computational particles) (three-dimensional ion-thruster plume simulation).

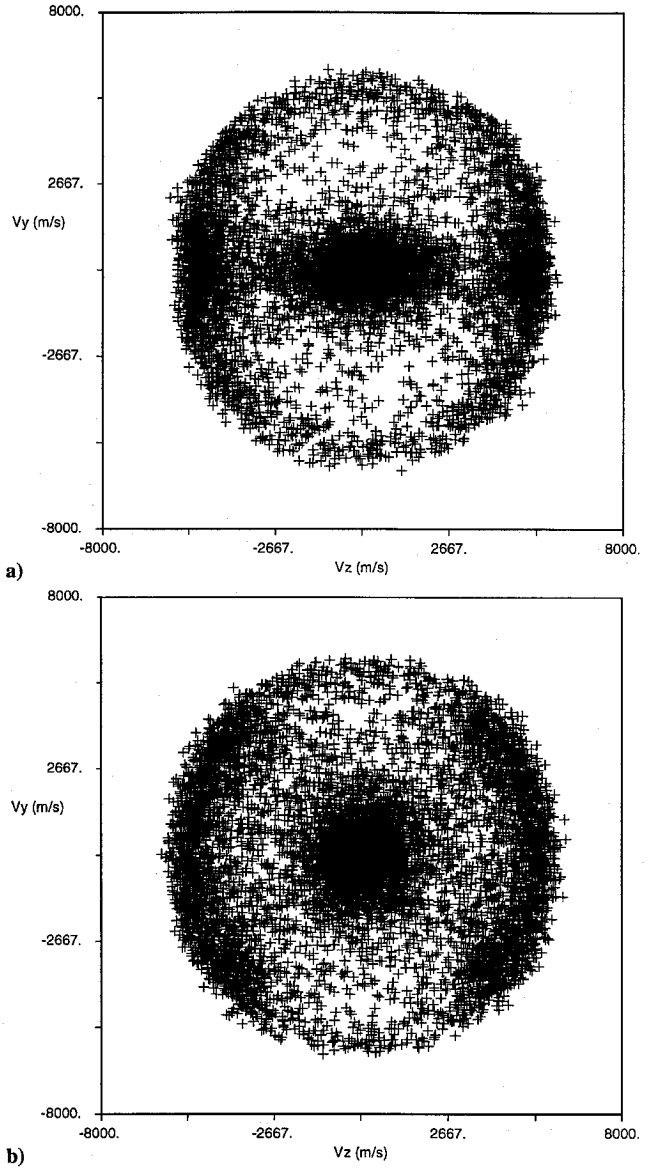

Fig. 7 Propellant CEX ions v_y–v_z velocity distribution plot for dual thrusters (random subset of all computational particles) with centerline separation distance of a) 10 cm and b) 17 cm (three-dimensional ion-thruster plume simulation).

outward (in the y–z plane), and back toward the spacecraft (backflowing in the $-x$ direction). The region between the two beams where CEX ions are trapped will be discussed later. Figure 4 displays a contour plot in the y–z plane 2 cm behind the thruster exit plane ($x = 8$ cm) showing the propellant CEX ion density. The contours clearly show the enhanced density on the sides of the spacecraft parallel to the axis joining the two thruster centers. The directional nature of the backflow within the y–z plane can be seen distinctly. Figure 5 shows an angular cut in the same y–z plane of the CEX ion current density sweeping from -90 deg ($-y$ axis) to 90 deg ($+y$ axis). At 0 deg ($+z$ axis), the current density is almost a factor of five greater than along the axis that joins the thruster centers.

It is useful to analyze the velocity distributions of the CEX ions. An examination of velocity phase space clearly shows how the propellant CEX ions are expelled radially from the beams. In Figs. 6 and 7, v_y–v_z phase plots are shown for both single and dual thruster operation, respectively. The y and z velocities of a randomly selected subset of all of the computational CEX ions (for all x) are shown. Thruster centerline separation was 10 cm in Fig. 7a and 17 cm in Fig. 7b. For the single thruster, the velocity distribution is symmetric as would be expected. With dual thruster operation, there are noticeable asymmetries in addition to distinct differences based on thruster separation distance. In Fig. 7a, the thermal region in the center, representing freshly born CEX ions created within the beam, is elongated in the v_z axis direction, compared to Fig. 7b, where the thrusters are separated by almost a thruster diameter more. However, in both dual thruster cases, the side regions along the v_z axis are more populated, although the distribution in Fig. 7b is formed along a broader arc.

The physical reason for the directional backflow is the potential structure within the beam that leads to trapping of the thermal propellant CEX ions. CEX ions from both beams that are transported into the potential well, between the two beams, are forced to leave where the potential hill falls down, and that is in the direction perpendicular to the axis joining the thruster centers. Figure 8 shows cuts of the predicted potential in the y–z plane 4 cm downstream of the thruster exits ($x = 14$ cm) along both the y and z axes that demonstrates that the potential structure is basically a saddle point. Figure 8a is from the 10-cm separation case, and Fig. 8b is from the 17-cm separation case. Since the thrusters are aligned along the y axis, there is a potential well along that axis, between the two beams, which traps CEX ions. Along the z axis there is only a potential hill. Thus, in this direction, more CEX ions leave leading to the directional component of the backflow. As the separation distance

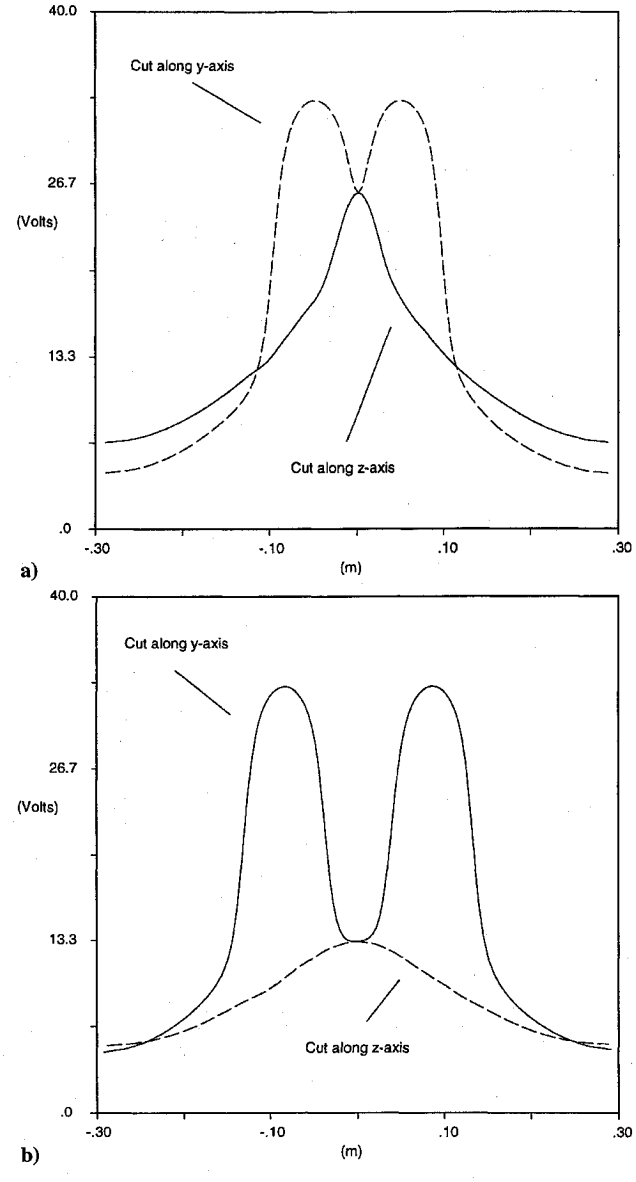

Fig. 8 Potential through beams along y and z axes at x = 14 cm; dual thrusters with centerline separation of a) 10 cm and b) 17 cm (three-dimensional ion-thruster plume simulation).

increases, the potential well increases, but the potential drop along the z axis decreases, and hence there is less focusing of ions along the axis perpendicular to the line joining the thruster centers. Instead, ions leave in a wider spread of y-axis velocities, which is clearly seen in the wide arcs in Fig. 7b.

Spacecraft/Grid Impingement Current

In addition to CEX ions being expelled out of the beams, a number of the CEX ions are trapped and attracted back toward the spacecraft in the region between the thrusters. In addition, a small percentage may actually increase the grid impingement current. Figure 3 shows the increased flow to the spacecraft from the region between the two beams where propellant CEX ions are trapped. The model in this study was not specifically designed to compute the grid impingement current because of the high resolution necessary at the grid hole level. However, comparisons with other models designed specifically for this purpose, as well as experimental data, show that our model gives reasonable estimates.[6] With dual thruster operation, the grid impingement current increased by 5% over single thruster operation.

NPE Sputtered Material

The backflow structure of sputtered grid material was examined with dual thruster operation. Figure 9 shows a v_y–v_z phase plot

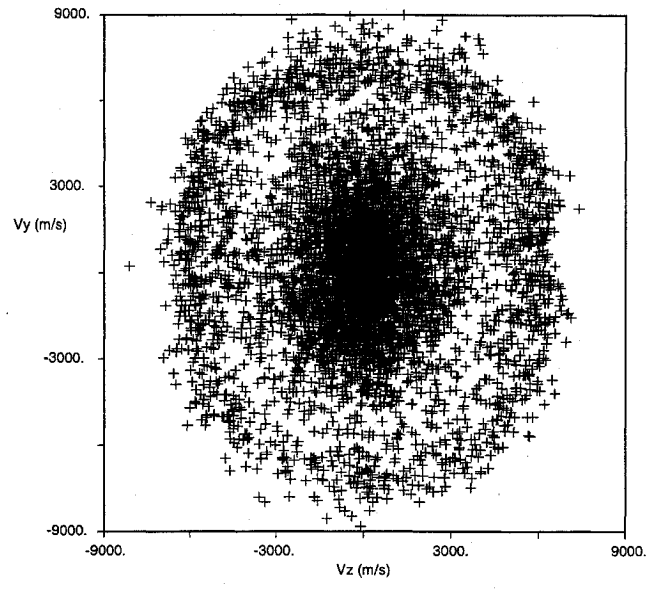

Fig. 9 Molybdenum ions v_y–v_z velocity distribution plot for 10-cm separation dual thruster case (random subset of all computational particles) (three-dimensional ion-thruster plume simulation).

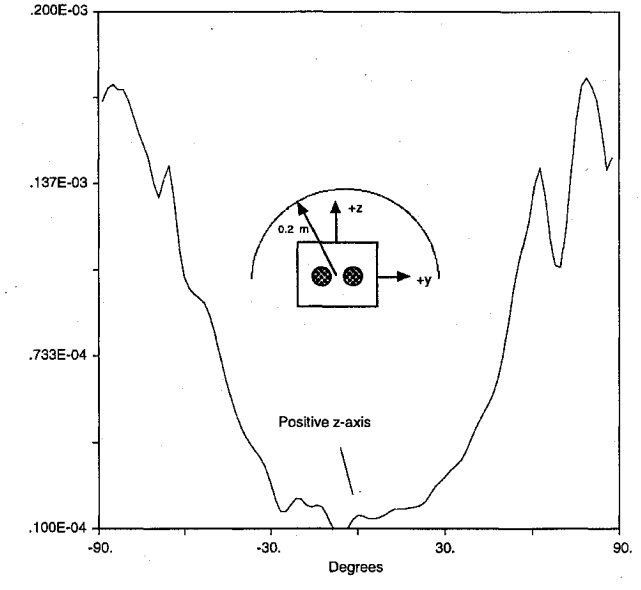

Fig. 10 Ratio of Mo to Xe CEX ion current density along angular arc in y–z plane 2 cm upstream of thruster exit plane (x = 8 cm) for 10-cm separation dual thruster case; arc radius is 20 cm (three-dimensional ion-thruster plume simulation).

of the sputtered molybdenum ions located at all x. Note that the elongation of the particle population along the v_z axis, as shown in Fig. 7 for the propellant CEX ions, is no longer present. Because the sputtered molybdenum ions are of much higher energy compared to the xenon CEX ions, they are not affected as much by the potential well between the beams. In fact, looking at the potential structures in Fig. 8, one sees that the net potential drop along the y axis is greater than along the z axis. Therefore, the velocity along that direction is higher for the molybdenum ions.

Last, it is interesting to look at the ratio of the molybdenum to xenon ion current density. In Fig. 10, this ratio is shown along an arc in the y–z plane 2 cm upstream of the thruster exits (x = 8 cm) from −90 deg (−y axis) to +90 deg (+y axis). This ratio is on the order of 10^{-5} at 0 deg, where the xenon CEX ion current density is the largest and the molybdenum CEX ion current density is the smallest, to over 10^{-4} at ±90 deg, where the opposite is true (compare with Fig. 5). These results indicate that minimum molybdenum deposition will take place along the z axis where maximum propellant CEX ion backflow is expected.

Conclusions

A three-dimensional model of two ion thruster plumes was developed and used to investigate the composite plume backflow. The CEX propellant backflow was computed, as well as the deposition of sputtered molybdenum from the thruster grids. The plume structure was found to be highly asymmetric as a result of a potential saddlepoint within the combined beams. This potential structure led to trapping of propellant CEX ions, and a preferential ejection in the direction perpendicular to the axis joining the thruster centers. Thus, the net backflow from dual thrusters is not a simple superposition of the backflow from two single thrusters. The separation between the thrusters plays a strong role, with decreased separation leading to more focused ejection. The influence of the potential structure on the sputtered grid material, however, is much less because of their much larger initial energies. Thus, there is greater flow along the axis joining the thruster centers. Hence, for sensitive surfaces, dual thruster orientation must be carefully considered so as to minimize the amount of backflow.

Acknowledgments

Support for this work was provided by the U.S. Air Force Office of Scientific Research under Contract F49620-93-1-0317. We would like to thank N. A. Gatsonis of Worcester Polytechnic Institute for useful discussions.

References

[1]Deininger, W. D., "Electric Propulsion Produced Environments and Possible Interactions with the SP-100 Power System," AIAA Paper 85-2046, Sept. 1985.

[2]Samanta Roy, R. I., Hastings, D. E., and Gatsonis, N. A., "Ion-Thruster Plume Modelling for Backflow Contamination," *Journal of Spacecraft and Rockets*, Vol. 33, No. 4, 1996, pp. 525–534.

[3]Samanta Roy, R. I., Hastings, D. E., and Gatsonis, N. A., "Numerical Study of Spacecraft Contamination and Interactions by Ion-Thruster Effluents," *Journal of Spacecraft and Rockets*, Vol. 33, No. 4, 1996, pp. 535–542.

[4]Samanta Roy, R. I., Hastings, D. E., and Taylor, S., "Three-Dimensional Plasma Particle-in-Cell Calculations of Ion Thruster Backflow Contamination," *Journal of Computational Physics* (to be published).

[5]Rapp, D., and Francis, W. E., "Charge Exchange Between Gaseous Ions and Atoms," *Journal of Chemical Physics*, Vol. 37, No. 11, 1962, pp. 2631–2645.

[6]Samanta Roy, R. I., "Numerical Simulation of Ion Thruster Plume Backflow for Spacecraft Contamination Assessment," Ph.D. Thesis, Dept. of Aeronautics and Astronautics, Massachusetts Inst. of Technology, Cambridge, MA, June 1995.

[7]Wang, J., Brophy, J., Liewer, P., and Murphy, G., "Modelling of Ion Thruster Plumes," AIAA Paper 95-0596, Jan. 1995.

[8]Kemp, R. F., Leudke, E. E., Hall, D. F., and Miller, W. D., "Effects of Electrostatic Rocket Material Deposited on Solar Cells," AIAA Paper 72-447, April 1972.

[9]Stuart, R. V., Wehner, G. K., and Anderson, G. S., "Energy Distribution of Atoms Sputtered from Polycrystalline Metals," *Journal of Applied Physics*, Vol. 40, No. 2, 1969, pp. 803–812.

[10]Birdsall, C. K., and Langdon, A. B., *Plasma Physics via Computer Simulation*, 2nd ed., Adam Hilger, Bristol, England, UK, 1991.

A. L. Vampola
Associate Editor